INTEROCULAR SYMMETRY OF PARAFOVEAL PHOTORECEPTOR CONE DENSITY DISTRIBUTION

MARCO LOMBARDO, MD, PHD,* GIUSEPPE LOMBARDO, MENG, PHD,†‡
DOMENICO SCHIANO LOMORIELLO, MD,* PIETRO DUCOLI, MD,* MARIO STIRPE, MD,*
SEBASTIANO SERRAO, MD, PHD*

Purpose: To investigate the variation and symmetry of cone density distribution along the nasal and temporal retina of fellow eyes.

Methods: An adaptive optics retinal camera (rtx1; Imagine Eyes) was used to obtain images of the parafoveal cone mosaic in 20 healthy subjects. Cone density was estimated at 250, 420, 760, and 1,300 μm eccentricity from the fovea along the nasal and temporal retina of both eyes in each subject. The coefficient of variation and the intraclass correlation coefficient were used to calculate the variation and absolute agreement of cone density between the same retinal eccentricity locations of fellow eyes, respectively.

Results: A considerable variation of cone density between subjects was found at all eccentricities along the nasal and temporal retina (intersubject coefficient of variation $\geq$ 11%, $P < 0.001$). The intrasubject variation of cone density was, however, moderate (coefficient of variation $\leq$ 13% in 95% of the subjects); a high agreement was, on average, found between the cone density estimates at the same eccentricity along the nasal and temporal retina of fellow eyes (intraclass correlation coefficient $\geq$ 0.86, $P < 0.001$).

Conclusion: Cone density follows a symmetrical distribution between fellow eyes. A systematic distribution of parafoveal cones between fellow eyes may provide an anatomical basis for the involvement of the photoreceptor layer in the first step of binocular spatial sampling.

RETINA 0:1–10, 2013

During the last decade, retinal imaging through adaptive optics (AO) has demonstrated reliable capability to image the living human retina at high resolution.[1,2] Data on populations of healthy eyes are fundamental to characterize the density, distribution, and appearance of the healthy photoreceptor cells in vivo. This would permit measurement of the normal ranges, which allows comparison with pathologic changes of photoreceptors, even in early stages of retinal diseases.

A few AO studies[3–6] have previously characterized the cone photoreceptor density distribution in small populations of healthy eyes. The in vivo measurements of cone density[3–6] have shown good agreement with histologic data from cadaver eyes,[7–11] with the exception of the foveal cone density data, that have been shown in vivo only in a limited number of cases because of the relatively low image quality of retinal images even when AO is used. In pivotal studies of the human photoreceptor mosaic, Curcio et al[7–9] found an average decrease in cone density from 199,000 cell/mm^2 at the foveal center to $\sim$35,000 cell/mm^2 at 0.5 mm and $\sim$20,000 cell/mm^2 at 1.0 mm eccentricity along the horizontal meridian in 7 cadaver eyes aged 27 years to 44 years. All the ex vivo and in vivo studies showed, at equivalent eccentricities, a 10% higher density of cones along the horizontal than the vertical meridian. Comparable cone density values were in general found at equivalent eccentricities between the nasal and temporal retina within 1 mm eccentricity from the fovea both in the ex vivo and in the in vivo studies.[6–9]

So far, there is no published comparison of the photoreceptors' spatial distribution between fellow eyes, with the exception of histologic data reported by Curcio

From the *Fondazione G.B. Bietti IRCCS, Rome, Italy; †CNR-IPCF Unit of Support Cosenza, University of Calabria, Rende, Italy; and ‡Vision Engineering, Rome, Italy.

None of the authors have any financial/conflicting interests to disclose.

Reprint requests: Marco Lombardo, MD, PhD, Fondazione G.B. Bietti IRCCS, Via Livenza 3, 00198 Rome, Italy; e-mail: mlombardo@visioeng.it

et al[7] in one subject. The in vivo study of intrasubject variability in cone density would add valuable information to better understand the normal characteristics of the cone mosaic. In this study, we investigated the variation and symmetry of cone density between fellow eyes in a population of healthy subjects.

Materials and Methods

Twenty healthy volunteer subjects participated in this study and gave written informed consent after a full explanation of the procedure. The protocol had the approval of the local ethical committee and adhered to the tenets of the Declaration of Helsinki. All subjects received a complete eye examination, including a subjective refraction, noncontact ocular biometry using partial coherence interferometry (IOL Master, Carl Zeiss Meditec Inc, Jena, Germany), and retinal imaging using a Heidelberg Retina SLO/OCT (Spectralis; Heidelberg Engineering GmbH, Heidelberg, Germany). Exclusion criteria for this study included any ocular or systemic diseases or previous eye surgery. All subjects had 20/20 or better best-corrected visual acuity.

A compact AO retinal camera prototype, the rtx1 (Imagine Eyes, Orsay, France), was used to image the photoreceptor layer.[12,13] The core components of the apparatus include a Shack–Hartmann wavefront sensor (HASO 32-eye; Imagine Optics, Orsay, France), a deformable mirror (MIRAO 52; Imagine Optics), and a low-noise high-resolution CCD camera (Roper Scientific, Tucson, AZ). The HASO 32 and MIRAO 52 work in closed loop: a proprietary algorithm measures the signal coming from the sensor and controls the deformable mirror to compensate the wavefront error of the eye. A modified Badal assembly corrects for −12 diopter (D)/+6 D of defocus.

Retinal Imaging Procedure

In this study, the AO imaging sessions were conducted after dilating the pupils with 1 drop each of 0.5% tropicamide and 10% phenylephrine hydrochloride. Fixation was maintained by having the patient fixate on the system's fixation target moved by the investigator to fixed retinal locations: in this study, the patient was instructed to fixate at 0°, 0.5°, 1.5°, 3°, 4.5°, and 6° eccentricity along the nasal and temporal retina, and a video camera monitored the subjects' pupil and eye movements.

A video (i.e., a series of 40 frames; 4° field size) was captured at each of the above retinal locations. After the acquisition, a program provided by the manufacturer correlated and averaged the captured image frames to produce a final image.[13] Distortions in images caused by eye movements and lid closure were eliminated (on average four frames per acquisition) to reduce noise artifacts and enhance the signal-to-noise ratio for subsequent image analysis.

Retinal Image Size Estimation

To correct for the differences in optical magnification and thus retinal image size between eyes with different axial lengths, we calculated the retinal magnification factor (RMF), using the nonlinear formula of Drasdo and Fowler and the Gullstrand schematic eye as model.[4,13–16] The biometric data of each eye (i.e., the anterior radius of curvature, anterior chamber depth, and axial length) were acquired using the IOL Master. When refractive correction was required, an additional correction factor was applied, that is, the spectacle corrected magnification factor (RMF_{corr}): it was estimated for each eye by consideration of the spherical equivalent refraction (corresponding to the trial lens added to the system). The spectacle vertex distance was set at 14 mm for all eyes. Radial and areal magnification factors were then computed for each eye. In this study, all cone densities and eccentricities were corrected based on this model.

Image Analysis

For each eye, the acquired images were stitched together to create a larger montage image of the photoreceptor mosaic using commercial software (Photoshop CS3 version 10; Adobe Systems, Inc, San Jose, CA), as shown in Figure 1. All montages were verified by comparison with the subject's Spectralis fundus images, as previously shown.[17] The foveal center for retinal coordinates was determined by finding the center of the image taken when the subject fixated on the yellow cross at 0° compared with the overlapping area of 2 images taken when the subject fixated on 0.5° nasal and 0.5° temporal angles.[17]

Cone density (in cones/mm^2) was measured at 250, 420, 760, and 1,300 μm eccentricities from the foveal center along the nasal and temporal retina, as shown in Figure 1. Cone identification was performed using ImageJ (version 1.45a; National Institutes of Health, Bethesda, MD). Filtering image processing was used to isolate signals corresponding to cone photoreceptors; local maxima were therefore identified in the filtered image, as shown in Figure 2[13]. Cone density for a given retinal eccentricity was composed by the data values among two 50×50-μm windows. Eccentricity was computed as the distance between the center of each window and the foveal center; manual editing was performed by the user to place the sampling windows in areas devoid of blood vessels.[13,17]

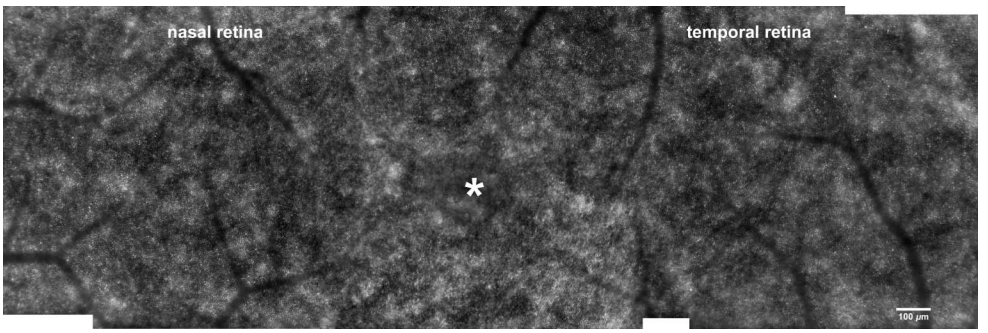

Fig. 1. Montage of the cone photoreceptor mosaic from the foveal center (asterisk) to 1,400 μm eccentricity along the nasal and temporal retina in Subject 19 (left eye). Cone density has been estimated in 50 × 50-μm sampling windows at 250, 420, 760, and 1,300 μm eccentricities along the nasal and temporal retina. Scale bar represents 100 μm.

The estimates of cone density were verified by three investigators (M.L., S.S., and G.L.) to minimize any potential cone under- or oversampling made by the automated software.

Statistics

Statistics were performed using the SPSS software (version 17.0; SPSS, Inc, Chicago, IL). Cone density data were expressed as mean ± standard deviation

C
O
L
O
R

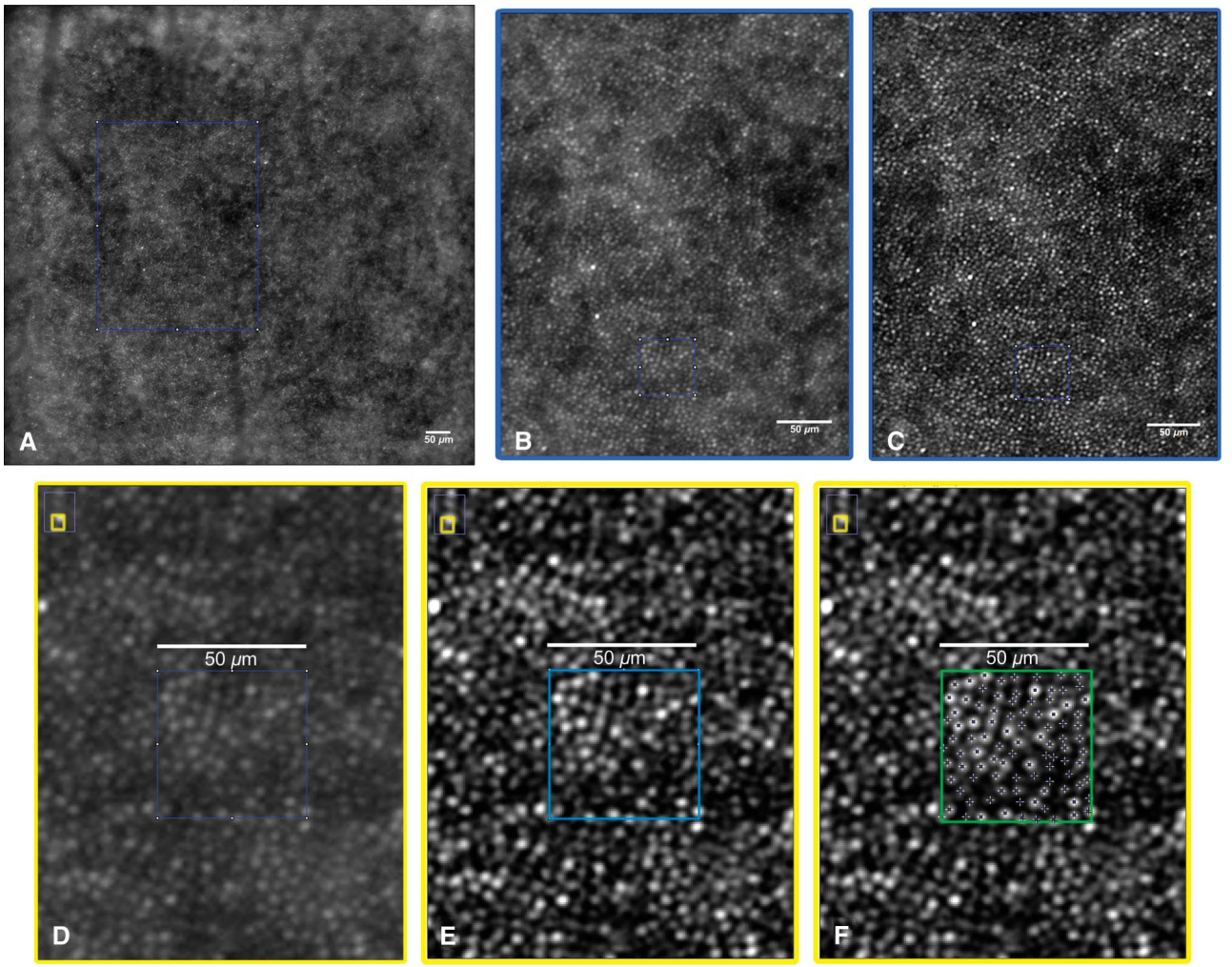

Fig. 2. A. Image of the cone mosaic centered at 1° temporal from the fovea (corresponding to 295 μm in this eye) in Subject 5. **B.** Subregion of the image shown in panel **A** centered at 250 μm eccentricity. **C.** The cone photoreceptor mosaic in the same region of interest after image processing that included background subtraction and contrast enhancing. The window represents the sampling area used for cone density measurements. **D–F.** The computation procedure of cone counting on a fixed 50 × 50-μm sampling window, before (**D**) and after (**E** and **F**) processing the image section is shown (the upper left inbox shows magnification with respect to images **B** and **C**). In this case, all the cones within the sampling window were identified. Overall, the number of cones added manually was between 0% and 9% across all images. Any cone whose center was located out of the rim of the sampling window was not included in the cone density estimate.

(SD). Differences between the spherical equivalent refraction (SEr) and axial length (AxL) of the right and left eyes were calculated using the one-way analysis of variance.

The error estimate of cone density measurements, performed on two 50 × 50-μm retinal sampling areas at the same eccentricity location by the automated algorithm, was calculated based on the intrasubject standard deviation (σ_w), that is, the common SD of repeated measurements. To get the common σ_w, we averaged the variances, that is, the squares of the SDs of the two repeated measures for each subject. The intrasubject SD was chosen as an index of measurement error, as discussed by Bland and Altmann.[18]

The coefficient of variation (CV) was used to analyze the variation of cone density at the same retinal eccentricity along the nasal and temporal regions of fellow eyes in each subject (intrasubject variation) and in the population study (intersubject variation). The intraclass correlation coefficient (two-way random effects model) was calculated to estimate the absolute agreement of cone density measurements between the same retinal eccentricity along the nasal and temporal regions of fellow eyes. The F-test was calculated to test the significance of both the variation and the absolute agreement between the variables of fellow eyes. A $P < 0.05$ was considered statistically significant for all the tests performed.

Results

Five men and 15 women participated in this study (mean age, 31.10 ± 4.70 years; range, 24–38 years). Spherical equivalent refractive errors ranged from +0.25 D to −5.75 D (SEr mean, −2.05 ± 2.03 D) with astigmatism less than –1.50 D. The mean SEr was −2.08 ± 2.12 D and –2.01 ± 1.95 D ($P > 0.05$) in the right and left eyes, respectively. The mean AxL was 24.15 ± 1.08 mm and 24.12 ± 1.09 mm ($P > 0.05$) in the right and left eyes, respectively. The subjects' characteristics are summarized in Table 1.

The estimated ranges for distance-to-angle and area-to-angle conversions were 0.267 to 0.307 mm/degree (mean ± SD, 0.281 ± 0.009 mm/degree) and 0.071–0.094 mm^2/degree^2 (mean ± SD, 0.079 ± 0.005 mm^2/degree^2), respectively.

The intrasubject standard deviation (σ_w) was <2,000 cones/mm^2 at 250 μm eccentricity; <1,800 cones/mm^2 at 460 μm; <1,600 cones/mm^2 at 760 μm; and <900 cones/mm^2 at 1,300 μm eccentricity. This means that the difference between 2 measurements for the same subject would be lower than 6% within 1,300 μm eccentricity. The number of cones missed by the automated algorithm, as determined by 3 observers, was between 0% and 9% across all images.

Cones were well resolved between 250 and 1,300 μm eccentricities in all the eyes (Figure 3). The average (±SD) cone density values of the population study and those of each subject are summarized in Table 2 (Figure 4).

Table 1. Patients' Characteristics and Retinal Image Size Correction Factor

Number of Subject	Gender	Age (Years)	AxL (mm)		SEr (D)		Radial RMF$_{corr}$ (mm/degree)	
			Right Eye	Left Eye	Right Eye	Left Eye	Right Eye	Left Eye
1	M	30	23.69	23.62	–0.25	–0.25	0.280	0.279
2	F	24	23.05	23.15	0.25	0.25	0.277	0.277
3	F	30	23.03	22.98	0	–0.25	0.274	0.273
4	M	38	22.61	22.67	–0.25	–0.25	0.267	0.268
5	F	24	23.48	23.47	–0.25	–0.25	0.277	0.277
6	F	32	23.44	23.32	–0.25	0	0.277	0.275
7	F	36	23.01	22.80	0	–0.25	0.274	0.271
8	M	36	23.80	23.98	0.25	0	0.285	0.287
9	F	31	24.72	24.44	–4.50	–4.50	0.283	0.280
10	M	38	26.14	25.93	–2.50	–2.25	0.289	0.287
11	F	34	25.49	25.23	–4.75	–4.50	0.292	0.289
12	F	24	26.29	26.63	–5.00	–5.00	0.302	0.306
13	F	25	24.42	24.42	–3.00	–3.00	0.274	0.274
14	F	32	24.24	23.78	–5.00	–3.50	0.278	0.273
15	F	35	25.21	25.31	–5.50	–5.25	0.289	0.290
16	F	32	23.89	24.01	–1.00	–1.50	0.279	0.281
17	F	31	23.83	23.80	–2.25	–2.25	0.286	0.286
18	F	28	25.30	25.22	–4.25	–4.00	0.290	0.290
19	M	36	24.35	24.41	–3.00	–3.00	0.278	0.278
20	F	26	23.05	23.10	–0.25	–0.25	0.274	0.274

F, female; M, male.

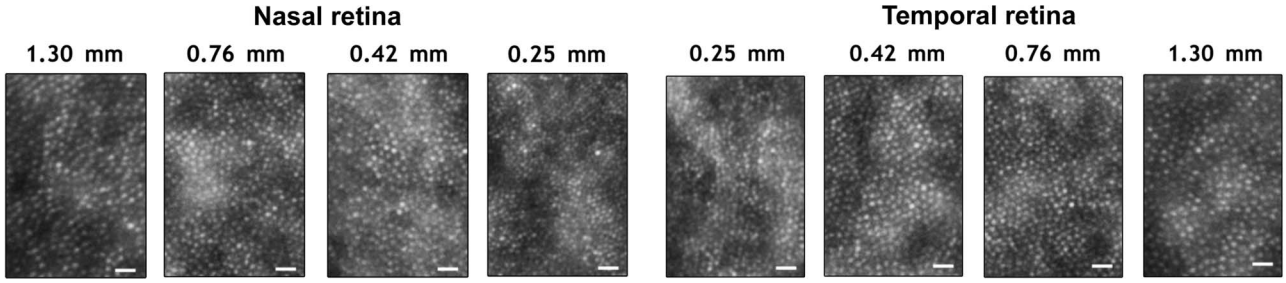

Fig. 3. Cone photoreceptor images (scale bars: 20 μm) of the regions of interest along the nasal and temporal retina in Subject 1. The images show the cone mosaic at each specified eccentricity. The cone photoreceptors are more densely packed at 250 μm eccentricity from the fovea than at increasing distances, as shown in Table 2 and Figure 4.

The CV of cone density between the same nasal and temporal retinal eccentricity locations of fellow eyes at 250 μm eccentricity was lower than 3% in 10 of 20 subjects; it was within 9% in all the subjects, except for Subject 5. The intrasubject variation of cone density slightly increased with increasing eccentricities at 420, 760, and 1,300 μm eccentricities; the intrasubject CV was within 9%, along both the nasal and temporal locations, in 18, 17, and 16 subjects, respectively. An intrasubject CV higher than 11% was found only in 1 subject at 420 and 760 μm eccentricity and in 4 subjects at 1,300 μm eccentricities. We found a considerable variation of cone density between subjects at all eccentricities ($P < 0.001$): the intersubject CV was within 17% (range, 12–17%) along the horizontal meridian within 1,300 μm eccentricity (Table 3).

A high degree of intraclass correlation was found between each retinal eccentricity along the nasal and temporal retina of fellow eyes: the intraclass correlation coefficient of the average cone density measurements between the same eccentricity locations of fellow eyes was 0.86 or higher ($P < 0.001$), as summarized in Table 3. We found a mean difference lower than 4% between the cone densities of fellow eyes, with a higher difference at 250 μm than at greater eccentricities.

Discussion

Adaptive optics retinal imaging has opened a new frontier for research in clinical ophthalmology,[19] permitting a real-time investigation of the cone photoreceptors. In this study, we evaluated the variation and symmetry of parafoveal cone density between fellow eyes in a population of healthy young adults. As far as we know, this is the first report on the intrasubject distribution of cone density. All previous studies have shown results on only one eye per subject and demonstrated a moderate-to-high interindividual variability in cone density distribution.[3–6] No previous work has attempted to estimate the intrasubject differences in cone density between eyes with the exception of a cadaver eye study by Curcio et al[7] in only 1 subject: the authors measured a mean 8% difference in both cones and rods densities between fellow eyes. The interocular differences between cone density, however, have not been measured as a function of retinal eccentricity, as done in the present work, rather than reported as global differences within the central 6-mm retina.

We found an average decline of cone density from ~51,000 cones/mm^2 at 250 μm eccentricity to ~14,000 cones/mm^2 at 1,300 μm eccentricity along the horizontal meridian. As in the previous studies,[3–6] we found marked interindividual differences in cone density; the CV of cone density was within 17% between 250 and 1,300 μm from the fovea. The intrasubject variation of cone density was, however, moderate: the CV was lower than 5% in 11 of 20 subjects (55% of the population) between the same nasal or temporal eccentricity locations of fellow eyes. In all the subjects, except for 1, the CV of cone density between the same retinal eccentricity locations of fellow eyes was lower than 13%. A high degree of absolute agreement was indeed found between the same retinal locations along the nasal and temporal retina of fellow eyes. In the parafoveal region, between 250 and 1,300 μm retinal eccentricities, cone density showed comparable values at the same eccentricities of fellow eyes: on average, we found differences lower than 4% between equivalent retinal locations of the nasal and temporal retina of fellow eyes.

The parafoveal cone density values shown in this study are in agreement with the previous studies where eyes of young adult populations (age range, 22–43 years; AxL range, 22.10–28.31 mm)[3–6] were imaged using an AO-SLO. On average, authors[3–6] found a cone density decline from ~59,000 cones/mm^2 at 0.27 mm to ~45,000 cones/mm^2 at 0.30 mm, ~35,000 cones/mm^2 at 0.50 mm, ~20,000 cones/mm^2 at 1.00 mm, and ~12,000 cones/mm^2 at 1.50 mm eccentricity from the fovea. In each of the previous studies, the cone density estimates between the nasal and temporal retina were ≤10% of each other within 1.8 mm eccentricity.

Table 2. Cone Density (Average, cones/mm^2) at each Retinal Location (Eccentricity from the Fovea, μm) Along the Horizontal Meridian (Nasal and Temporal Retina) in Both Eyes of the Population Study

Right Eye									Left Eye							
Temporal Retina				Nasal Retina				Number of	Temporal Retina				Nasal Retina			
1,300 μm	760 μm	420 μm	250 μm	250 μm	420 μm	760 μm	1,300 μm	Subject	1,300 μm	760 μm	420 μm	250 μm	250 μm	420 μm	760 μm	1,300 μm
17,801	36,904	49,495	58,192	56,442	48,627	36,470	19,538	1	17,367	34,533	47,627	58,613	57,376	47,758	34,299	17,801
19,998	30,826	43,851	58,169	57,310	46,456	30,826	22,143	2	20,406	31,194	42,417	48,758	50,193	41,917	30,826	23,011
17,459	37,809	48,679	63,330	62,857	46,316	36,863	16,151	3	17,459	37,336	50,233	56,140	60,494	49,682	37,336	17,363
14,958	36,662	52,169	62,480	60,898	44,942	37,695	14,975	4	14,360	34,524	43,934	54,824	53,343	44,946	34,080	14,348
10,049	23,879	39,509	51,232	50,061	39,509	24,313	9,865	5	11,788	28,655	37,338	50,179	51,298	39,075	30,392	12,225
11,288	28,655	44,285	53,403	52,968	43,851	28,221	11,420	6	13,120	30,826	40,680	52,200	53,837	42,548	32,128	13,895
12,800	28,397	35,200	48,807	48,396	40,800	32,398	12,850	7	15,400	30,398	39,603	49,250	49,261	40,000	30,807	14,900
11,175	34,500	43,007	56,240	57,658	44,425	33,083	10,952	8	10,425	33,083	43,007	56,179	59,603	43,953	33,555	10,398
16,400	28,400	37,600	50,002	48,400	39,200	28,402	15,603	9	17,064	30,826	39,312	50,798	48,193	38,207	32,128	16,196
15,540	28,860	33,670	42,810	43,290	36,260	28,860	14,855	10	16,040	31,820	36,500	42,310	42,920	38,110	33,540	15,005
13,719	26,065	32,739	42,527	43,556	33,581	26,065	13,754	11	14,780	27,380	36,950	47,140	46,990	38,570	27,620	15,340
9,729	20,411	28,385	43,988	43,669	28,066	20,411	9,848	12	10,020	19,915	25,860	43,341	42,902	27,346	20,510	10,039
14,651	34,028	43,425	59,076	60,494	41,590	33,555	14,233	13	13,807	31,192	48,624	60,912	60,049	48,074	32,610	14,178
14,328	30,826	39,075	46,448	46,456	36,036	30,023	13,959	14	13,843	33,555	40,144	51,987	50,124	39,227	34,273	15,841
13,930	29,600	38,960	46,990	46,980	38,960	27,010	14,190	15	13,970	26,270	34,650	44,700	43,890	33,890	25,530	13,370
10,252	26,918	39,509	51,666	48,522	39,075	26,500	10,202	16	10,840	26,798	36,803	43,997	45,300	38,007	27,200	10,495
11,660	29,528	35,740	48,713	49,982	38,235	29,459	11,144	17	12,310	27,425	39,738	49,934	48,313	37,740	28,762	12,110
15,100	28,455	34,590	43,820	45,210	34,990	28,060	15,350	18	15,649	31,374	37,973	44,215	44,665	37,233	30,302	14,811
14,198	28,992	39,407	53,564	51,458	37,730	27,813	13,948	19	14,237	28,251	39,307	48,707	48,271	38,170	26,018	14,017
14,513	27,455	35,183	45,327	45,101	32,714	24,865	13,893	20	14,554	26,238	33,074	42,155	42,550	33,102	25,648	13,759
13,952	29,859	39,724	51,339	50,986	39,567	29,545	13,943	Population	14,372	30,080	39,688	49,847	49,928	39,872	30,378	14,460

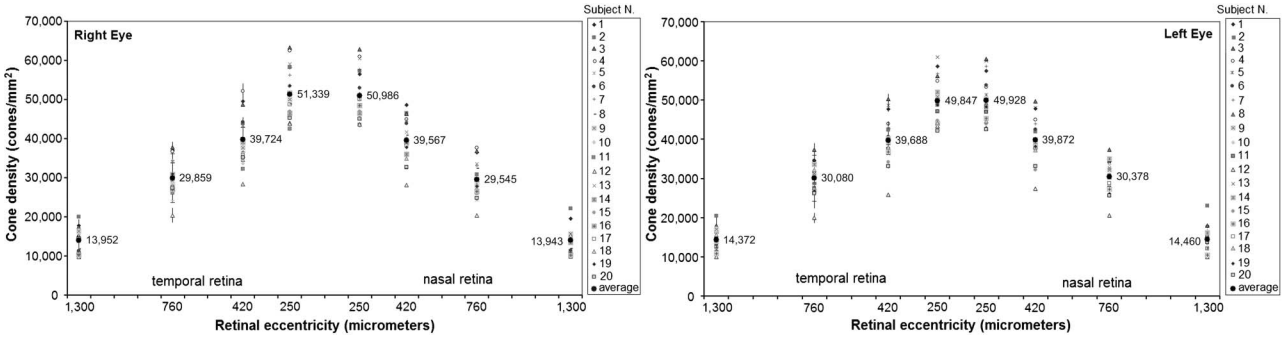

Fig. 4. The average and individual cone density estimates (in cones/mm^2) along the nasal and temporal retina of the right and left eyes are shown. The numbers show the average cone density values at each eccentricity location. For average values, the vertical bar represents 1 SD from the mean; for the single values, the bar represents the SD of two repeated measurements.

Histology studies, however, have shown that, at eccentricities greater than 2.0 mm from the foveal center, the cone density is more than 10% higher in the nasal than in the temporal retina.[6,10] The slight discrepancies between AO studies could depend on the inclusion of subjects with different ages or eyes with different axial lengths and refractive corrections, on the model eye used to estimate the retinal image size and the sampling window area used to count cones, as shown in Table 4 and described in the Appendix. In this study, the eyes with longer axial length showed a lower cone density and a higher SD from the mean compared with emmetropic eyes at each eccentricity, as previously found.[3,4,13] A detailed analysis of the differences in cone density in relation to axial length was not reported here because it was subject of a previous work.[13]

In this study, cone photoreceptors were counted within 2 windows of 50 × 50 μm.[13,17] We based our method on the results of a previous work by Hirsch and Miller[20]: the authors demonstrated that a 56 × 56-μm area was less subject to error than smaller window sizes when estimating cone density across increasing eccentricity from the fovea. Inaccuracies could be ascribed to the analytical method when fewer cells are identified in the sampling window. We made sure not to perform cone photoreceptor counting on regions with vessels or defects in the image quality: an underestimation of density may indeed occur when regions of missing data (e.g., blood vessels or dark areas likely because of defects in the image quality) are present in the sampling window. Previous authors also used a 50 × 50-μm sampling window to locate cone photoreceptor positions,[6] further showing a high repeatability in cone density estimates taken 6 months apart at the same retinal location. Larger fixed window sizes or adaptive sampling windows (i.e., adjusted to contain a constant number of cones across eccentricities) have also been used.[3,5,21,22]

We quantified the cone density measurement error of the automated algorithm, showing an estimate error lower than 6% within 1,300 μm eccentricity along the horizontal retinal meridian. There are two previous studies[1,23] that reported statistics for repeated measures of cone density taken at the same retinal location. Both provided an estimate error in cone density measurements between 6.1% and 7.4% within 0.70° eccentricity, favorably comparing with what shown in our study. The error in cone density estimates was attributed to cone selection, magnification error, distortion in cone images, selection of the region of interest, sampling area, and precise alignment of images from each imaging session.

The variation of intrasubject cone density distribution was taken relative to fixation, under assumption that the steady fixation region was located at the foveal center in all the eyes: however, no measurement of the steady fixation was done to confirm this assumption because we were not able to resolve the smallest cones at the foveola. Previous studies[4,24] found that the center of fixation could deviate, on average, 18 ± 11 μm from

Table 3. Coefficient of Variation and Intraclass Correlation Coefficient (ICC for Average Measures with 95% Confidence Interval) Between the Same Retinal Eccentricity Locations Along the Horizontal Meridian (Nasal and Temporal Retina) of Fellow Eyes

	Temporal Retina				Nasal Retina			
	250 μm	420 μm	760 μm	1,300 μm	250 μm	420 μm	760 μm	1,300 μm
Intersubject CV*	12%	14%	14%	17%	12%	13%	14%	17%
ICC*	0.86	0.89	0.89	0.93	0.93	0.90	0.88	0.92
95% CI of ICC	0.66–0.95	0.73–0.96	0.72–0.96	0.82–0.97	0.83–0.97	0.75–0.96	0.71–0.95	0.79–0.97

*F-test: $P < 0.001$.

Table 4. Cone Density Estimates in Histology and AO Retinal Imaging Studies Taken at Increasing Eccentricities from the Foveal Center

Work	Number of Subjects; Age (Range Years); AxL (Range, mm); Sampling Window Area (μm or pixels); Model Eye	Cone Density (Average, cones/mm^2) as a Function of Retinal Eccentricity (Range, μm) Along the Horizontal Meridian			
		From 250 to 360 μm	From 400 to 540 μm	From 720 to 890 μm	From 1,000 to 1,350 μm
Curcio et al[7]	7; 27–44; AxL not reported; variable sampling windows; anatomical schematic eye	Nasal/temporal: 60,000–55,000	Nasal/temporal: 40,000	Nasal/temporal: 26,000	Nasal/temporal: 20,000
Li et al[4]	18; 23–43; 22.9–28.3 mm; adaptive windows (adjusted to contain 150 cones); Gullstrand schematic eye model	All meridians: 60,000–45,000	Not reported	Not reported	Not reported
Chui et al[3]	11; 21–31; 22.8–27.5 mm; 150 $\times$ 150-pixels window; standard reduced eye model	Not reported	Nasal/temporal: 41,000	Nasal/temporal: 27,000	Nasal/temporal: 15,000
Chui et al[5]	4; 24–54; AxL L not reported; 22 $\times$ 22-μm window; model eye not reported	Not reported	Temporal: 30,000	Not reported	Temporal: 15,000
Song et al[6]	10; 22–35; 22.1–26.1 mm; 50 $\times$ 50-μm window; Indiana model eye	Nasal: 59,700–50,000; temporal: 59,200–50,500	Nasal: 43,700–37,800; temporal: 41,200–37,300	Nasal: 29,100–24,200; temporal: 28,100–24,100	Nasal: 19,100–16,800; temporal: 19,900–16,300
This study	20; 24–38; 22.6–26.6 mm; 50 $\times$ 50-μm window; Gullstrand schematic eye model	Nasal/temporal: 51,339–49,847	Nasal/temporal: 39,872–39,567	Nasal/temporal: 30,378–29,545	Nasal/temporal: 14,460–13,943

the foveal center; Møller et al[25]. found that the preferred retinal locus of fixation was symmetrically along the horizontal meridian between fellow eyes in healthy subjects, although with interindividual variations. By laterally displacing the center of our sampling window by 18 μm, the potential error in our eccentricity-dependent cone density measurements has been estimated to be $<$1,000 cones/mm^2 and 500 cones/mm^2 at 250 and 1,300 μm eccentricity, respectively.

The interocular symmetry of microscopic anatomical properties of the retina may have direct consequences for visual function. The highly ordered and systematic architecture of the cone mosaic in the parafoveal region between fellow eyes could be the result of an evolutionary process creating appropriate location information for binocular spatial sampling. Bilateral interaction of the eye's optical components has been thoroughly investigated: symmetry of corneal topography and ocular wavefront aberrations between the right and left eyes has been demonstrated in various clinical and experimental studies.[26–30] Moreover, cone directionality apodization (the Stiles–Crawford effect)[26,31–33] has also shown symmetry between fellow eyes, albeit with interindividual differences. The systematic process underlying the cone density distribution across the foveal region between fellow eyes may provide a functional basis for the initial extraction of binocular spatial information.

Key words: adaptive optics, cone photoreceptors, retinal anatomy, retinal histology.

Acknowledgment

The authors are grateful to Dr. Nicholas Devaney (Applied Optics Group, NUI, Galway, Ireland) for his valuable comments and revision of the manuscript.

References

1. Garrioch R, Langlo C, Dubis AM, et al. Repeatability on in vivo cone density and spacing measurements. Optom Vis Sci 2012;89:632–643.
2. Pallikaris A, Williams DR, Hofer H. The reflectance of single cones in the living human eye. Invest Ophthalmol Vis Sci 2003;44:4580–4592.
3. Chui TYP, Song H, Burns S. Individual variations in human cone photoreceptor packing density: variations with refractive error. Invest Ophthalmol Vis Sci 2008;49:4679–4687.
4. Li KY, Tiruveedhula P, Roorda A. Intersubject variability of foveal cone photoreceptor density in relation to eye length. Invest Ophthalmol Vis Sci 2010;51:6858–6867.
5. Chui TYP, Song H, Burns S. Adaptive-optics imaging of human cone photoreceptor distribution. J Opt Soc Am A Opt Image Sci Vis 2008;25:3021–3029.
6. Song H, Chui TYP, Zhong Z, et al. Variation of cone photoreceptor packing density with retinal eccentricity and age. Invest Ophthalmol Vis Sci 2011;52:7376–7384.
7. Curcio CA, Sloan KR, Kalina RE, Hendrickson AE. Human photoreceptor topography. J Comp Neurol 1990;292:497–523.
8. Curcio CA, Sloan KR. Packing geometry of human cone photoreceptors: variation with eccentricity and evidence of local anisotropy. Vis Neurosci 1992;9:169–180.
9. Curcio CA, Sloan KR, Packer O, et al. Distribution of cones in human and monkey retina: individual variability and radial asymmetry. Science 1987;236:579–582.
10. Østerberg GA. Topography of the layer of rods and cones in the human retina. Acta Ophthalmol 1935;13:1–97.
11. Jonas JB, Schneider U, Naumann GOH. Count and density of human retinal photoreceptors. Graefes Arch Clin Exp Ophthalmol 1992;230:505–510.
12. Zacharria M, Lamory B, Château N. Biomedical imaging: new view of the eye. Nat Photon 2011;5:24–26.
13. Lombardo M, Serrao S, Ducoli P, Lombardo G. Variations in the image optical quality of the eye and the sampling limit of resolution of the cone mosaic with axial length in young adults. J Cataract Refract Surg 2012;38:1147–1155.
14. Drasdo N, Fowler CW. Non-linear projection of the retinal image in a wide-angle schematic eye. Br J Ophthalmol 1974; 58:709–714.
15. Coletta NJ, Watson T. Effect of myopia on visual acuity measured with laser interference fringes. Vision Res 2006;46:636–651.
16. Bennett AG, Rudnicka AR, Edgar DF. Improvements on Littmann method of determining the size of retinal features by fundus photography. Graefes Arch Clin Exp Ophthalmol 1994;232:361–367.
17. Lombardo M, Lombardo G, Ducoli P, Serrao S. Adaptive optics photoreceptor imaging. Ophthalmology 2012;119:1498–198.e2.
18. Bland JM, Altman DG. Measurement error proportional to the mean. BMJ 1996;313:106.
19. Godara P, Dubis AM, Roorda A, et al. Adaptive optics retinal imaging: emerging clinical applications. Optom Vis Sci 2010; 87:930–941.
20. Hirsch J, Miller WH. Does cone positional disorder limit resolution? J Opt Soc Am A 1987;4:1481–1492.
21. Li KY, Roorda A. Automated identification of cone photoreceptors in adaptive optics retinal images. J Opt Soc Am A Opt Image Sci Vis 2007;24:1358–1363.
22. Xue B, Choi SS, Doble N, Werner JS. Photoreceptor counting and montaging of en-face retinal images from an adaptive optics fundus camera. J Opt Soc Am A Opt Image Sci Vis 2007;24:1364–1372.
23. Talcott KE, Ratman K, Sundquist SM, et al. Longitudinal study of cone photoreceptors during retinal degeneration and in response to ciliary neurotrophic factor treatment. Invest Ophthalmol Vis Sci 2011;52:2219–2226.
24. Putnam NM, Hofer HJ, Doble N, et al. The locus of fixation and the foveal cone mosaic. J Vis 2005;5:632–639.
25. Møller F, Laursen ML, Sjølle AK. Fixation topography in normal test persons. Graefes Arch Clin Exp Ophthalmol 2006;244:577–582.
26. Marcos S, Burns SA. On the symmetry between eyes of wavefront aberration and cone directionality. Vision Res 2000;40:2437–2447.
27. Myrowitz EH, Kouzis AC, O'Brien TP. High interocular corneal symmetry in average simulated keratometry, central corneal thickness, and posterior elevation. Optom Vis Sci 2005;82:428–431.
28. Lombardo M, Lombardo G, Serrao S. Interocular high-order corneal wavefront aberration symmetry. J Opt Soc Am A Opt Image Sci Vis 2006;23:777–787.
29. Wang L, Santaella RM, Booth M, Koch DD. Higher-order aberrations from the internal optics of the eye. J Cataract Refract Surg 2005;31:1512–1519.

30. Jimenez Cuesta JR, Anera RG, Jimenez R, Salas C. Impact of interocular differences in corneal asphericity on binocular summation. Am J Ophthalmol 2003;135:279–284.
31. He JC, Marcos S, Burns SA. Comparison of cone directionality determined by psychophysical and reflectometric techniques. J Opt Soc Am A Opt Image Sci Vis 1999;16:2363–2369.
32. Applegate RA, Lakshminarayanan V. Parametric representation of Stiles-Crawford functions: normal variation of peak location and directionality. J Opt Soc Am A Opt Image Sci Vis 1993;10:1611–1623.
33. Lombardo M, Lombardo G. Wave aberration of human eyes and new descriptors of image optical quality of the eye. J Cataract Refract Surg 2010;36:313–331.

Appendix

A model is needed to correct for the differences in retinal image size between eyes with different AxL and SEr to minimize errors in cone density measurement (when expressed in cones/mm^2), as previously shown.[3,4,6,13–15] In this study, we found 0.277 ± 0.005 mm/degree as the average radial magnification factor (RMF_{corr}) in emmetropes (i.e., when the SEr was ±0.50 D and the AxL ranged between 23.00 and 24.00 mm) and 0.286 ± 0.008 mm/degree in moderate myopes (SEr, −5.50 D or less and AxL range, 24.01–26.70 mm) to estimate cone density between 0.25 and 1.30 mm from the fovea. Our data were compared with two previous studies.[3,15] In the first study, Li et al[4] found an average radial RMF_{corr} of 0.283 mm/degree in 6 emmetropic eyes (AxL ranging between 23.40 and 24.48 mm) and 0.312 mm/degree in 5 moderately myopic eyes (SEr ranged from −2.25 D to −5.50 D; AxL ranged between 24.54 and 25.73 mm). In the second study, Coletta and Watson[15] found an average radial RMF_{corr} of 0.276 mm/degree in emmetropes and 0.295 mm/degree in moderate and high myopes (up to −16 D). The slight discrepancies between the magnification factors could be mainly because of the different schematic eye model (Gullstrand or modified Gullstrand eye) and the different spectacle vertex distance (11 or 14 mm) used to calculate the retinal image size.